Characteristics of dust voids in a strongly coupled laboratory dusty plasma

Article *in* Physics of Plasmas · May 2018

DOI: 10.1063/1.5029338

7 authors, including:

Yoshiko Bailung
Institute of Advanced Study in Science and Technology

Tonuj Deka
Institute of Advanced Study in Science and Technology

Abhijit Boruah
Institute for Plasma Research

Sumita K Sharma
Institute of Advanced Study in Science and Technology, Guwahati, India

Characteristics of dust voids in a strongly coupled laboratory dusty plasma

Yoshiko Bailung, T. Deka, A. Boruah, S. K. Sharma, A. R. Pal, Joyanti Chutia, and H. Bailung

Citation: Physics of Plasmas **25**, 053705 (2018); doi: 10.1063/1.5029338
View online: https://doi.org/10.1063/1.5029338
View Table of Contents: http://aip.scitation.org/toc/php/25/5
Published by the American Institute of Physics

PHYSICS OF PLASMAS 25, 053705 (2018)

Characteristics of dust voids in a strongly coupled laboratory dusty plasma

Yoshiko Bailung, T. Deka, A. Boruah, S. K. Sharma, A. R. Pal, Joyanti Chutia, and H. Bailung[a)]

Basic and Applied Plasma Laboratory Physical Sciences Division, Institute of Advanced Study in Science and Technology, Paschim Boragaon, Garchuk, Guwahati 35, Assam, India

(Received 13 March 2018; accepted 23 April 2018; published online 9 May 2018)

A void is produced in a strongly coupled dusty plasma by inserting a cylindrical pin (~0.1 mm diameter) into a radiofrequency discharge argon plasma. The pin is biased externally below the plasma potential to generate the dust void. The Debye sheath model is used to obtain the sheath potential profile and hence to estimate the electric field around the pin. The electric field force and the ion drag force on the dust particles are estimated and their balance accounts well for the maintenance of the size of the void. The effects of neutral density as well as dust density on the void size are studied. *Published by AIP Publishing.* https://doi.org/10.1063/1.5029338

I. INTRODUCTION

A complex plasma (also known as a colloidal or dusty plasma) consists of electrons, ions, and a dispersed phase of microparticles (called dust grains) with sizes ranging from micron to sub-micron. Dust is naturally abundant in space plasmas such as planetary rings, comets, nebulae, etc., also found in plasmas used for industrial applications and in thermonuclear fusion devices like tokamaks.[1–4] Because of such abundance, research in dusty plasmas have attained immense interest during the last few decades.[5–10] Dust, when exposed to the plasma environment, immediately becomes charged by collecting electrons and ions. Laboratory study of such charged dust particles in plasma has introduced a great variety of new phenomena associated with waves and instabilities[7,11–15] and has also provided a number of interesting dynamical structures, such as plasma crystal formation,[16–18] Mach cones,[19,20] and voids.[21–26]

The spontaneous formation of voids in a dusty plasma experiment is fairly robust and has attracted great interest. Void is a dust free region inside a dust cloud that is frequently encountered in dusty plasma experiments performed under microgravity conditions as well as in ground based laboratory conditions. Study of voids in dusty plasma dates back to 1996 when Praburam and Goree[21] first reported the appearance of a spoke-shaped, dust free region in a cloud of 100 nm carbon particles in a radio-frequency (rf) discharge formed between parallel plate graphite electrodes. This dust free region, which is called as the "great void" mode, rotates azimuthally in the discharge and appears only when the dust particles had grown to a sufficiently large size. Samsonov and Goree[22] studied this void structure in detail and observed that as dust particles in a sputtering plasma grew in diameter up to about 120 nm, the void was developed by a sudden onset of a filamentary mode in which the ionization rate and dust number density were both modulated. In microgravity experiments also, centimeter-size stable dust voids were observed by Morfill *et al.*[23] which occurred without any initial turbulent phase. It was then Rothermal *et al.*[24] who observed voids with micrometer sized particles for the first time by compensating the effect of gravity with thermophoretic force. The onset and growth of a dust void are also investigated in a radio-frequency (rf) sheath of a capacitively coupled argon plasma by injecting micrometer sized dust particles from outside.[27] A circularly symmetric void emerges and grows with increasing rf power and pressure in the central region of the dust cloud levitating in the sheath. The theory of spontaneous void formation has been attributed to a dust density perturbation which produces a positive potential with respect to the surrounding plasma which in turn gives rise to an electric field that points outward from the region of dust depression.[22,28] Due to this electric field, the negatively charged dust particles are subjected to an inward electric force and the ions experience an outward drift resulting in an outward ion drag force on the dust particles. The balance of the two opposing forces determines the void boundary.

The characteristics of the void structure and its physics have also been studied by inserting electrically floating metal objects into a dusty plasma cloud.[29,30] Thompson *et al.*[29] studied the interaction of a tungsten wire (1.6 mm in diameter) with a dusty plasma formed in a dc discharge. In this case, the electric field is directed inward due to the negative electrostatic potential on the floating wire, which pushes the negatively charged particles outward. Assuming a linearized Boltzmann relation for dust density, they stated that the space around the wire will be devoid of dust out to a radius where the potential had fallen from the wire floating potential to the thermal energy of the dust. At the floating condition of the wire, the void formed is about ~1 cm. Another experiment was also performed by Thomas, Jr. *et al.*[30] where they produced a probe induced void in an argon dc glow discharge plasma. The void formed is ~1 cm diameter with a probe size of 0.2 mm diameter. The void characteristics and its physics were studied by applying different bias voltages to the probe. They concluded that the void was formed due to the balance of the outward electric field force and the inward ion drag force (due to the inward ion drift). Both these experiments were performed in dc discharge plasma.

a)hbailung@yahoo.com

In a recent study, Yaroshenko *et al.*[31] found that balance between electric field force and ion drag force has a strong dependence on the dust density in a complex plasma.

In this paper, we present an experiment, in which a void is formed by inserting a cylindrical pin of 0.1 mm diameter into a micron sized dust cloud formed in a capacitively coupled rf discharge plasma. We study void characteristics by varying the bias voltages to the pin below the plasma potential. The effect of neutral pressure and dust density on the size of the void is also discussed.

II. EXPERIMENTAL SETUP

The experiment is performed in a cylindrical glass chamber of 100 cm length and 15 cm diameter.[15] A schematic diagram of the experimental setup is shown in Fig. 1(a). Discharge is produced by applying radiofrequency power ∼5 to 10 W at a frequency of 13.56 MHz from an rf power generator to a thin aluminum strip placed on the outer surface of the glass chamber. A rectangular graphite plate 30 cm (length) × 14.5 cm (breath) × 0.2 cm (thickness) is kept horizontally inside the chamber with vertical fencing at both ends. The plate is kept electrically grounded. The vertical fences are stainless steel strips of 1.5 cm height, which provide axial confinement to the dust particles. The chamber is first evacuated down to a pressure of ∼0.2 Pa and is then filled with argon gas to attain a working pressure in the range of ∼(2.0–6.0) Pa. Dust grains used in this experiment are gold coated silica particles ∼5 μm in diameter and mass density ∼2.6 g cm^{-3}. A piezoelectric buzzer filled with micron dust is fitted below the graphite plate. Dust particles are dispersed into the plasma through a small hole (∼0.3 cm in diameter) made on the plate just above the buzzer by applying a small dc voltage (∼6 to 10 V) to the buzzer. Immersed into the plasma, the particles acquire a large amount of negative charge, due to the inflow of plasma electrons and ions.

The charged dust particles levitate in the plasma sheath boundary region (∼0.7 cm above the graphite plate) by balancing the upward sheath electrostatic force over the plate and the downward gravitational force. The levitating dust cloud extends horizontally over the whole area of the plate (except the sheath region). Levitated dust particles are illuminated by the laser light scattering technique using a horizontal sheet of green laser light (532 nm, 30 mW). The vertical extent of the particle cloud is only 2 layers. All the measurements and calculations are done in a single layer (illuminated by thin laser sheet). A high resolution camera is used to record still images and/or video recordings. A cylindrical pin made of tungsten and 100 μm in diameter is placed vertically above the graphite plate. A small ceramic tube (∼0.2 cm in diameter) is used to insulate the pin with the plate. A smaller diameter of the pin is used to reduce the local disturbance. The vertical length of the pin above the plate is 1.5 cm so that ∼0.8 cm of the pin is exposed to bulk plasma. The sheath above the grounded plate is ∼0.7–1.0 cm. Near to the pin, the dust particles experience an outward electrostatic force in a horizontal plane, due to the negative floating potential of the pin with respect to the plasma. As the sheath is formed, there is also an ion drift towards the pin, giving rise to the ion drag force on the dust particles which is directed radially inward with the pin as a center. The interplay between these two forces generates a circular void around the pin. At the void boundary, these two forces equate each other. A typical image of the circular void formed around the pin at floating potential is shown in Fig. 1(b). The illuminated point at the center is the reflection of laser light from the pin. When argon gas pressure is slowly varied from 0.2 Pa to 6.0 Pa, phase transition of the dusty plasma (from fluid to an ordered lattice structure) is clearly observed. In this experiment, the Coulomb coupling parameter Γ (which is the ratio of inter-dust Coulomb potential energy to the average dust thermal energy) lies in the range $1 \leq \Gamma < \Gamma_c$ (where Γ_c is the critical value of Coulomb coupling parameter above which strongly coupled dusty plasma attains the crystalline state).[17] So, the dusty plasma in the present experiment is in a strongly coupled fluid state. An rf compensated cylindrical Langmuir probe made up of tungsten wire of 1 cm length and 0.02 cm diameter is used to measure the different plasma parameters. Typical values of the measured plasma parameters are as follows: ion densities (n_i) $\sim 10^8$ cm^{-3}, electron temperature $T_e \sim$ (5–6) eV, dust charge $Q_d \sim (2\text{–}3) \times 10^4$ electron charge, and dust density n_d (calculated from the interparticle distance) $\sim (10^2\text{–}10^3)$ cm^{-3}. Dust particles and plasma ions are considered to be at room temperature.

III. EXPERIMENTAL RESULTS AND DISCUSSION

Figure 2 shows typical images of the circular dust void when the pin is biased at different voltages ($V_b = \sim +38$ V to -30 V) at a constant neutral pressure of 4.6 Pa. The other parameters such as dust density (∼800 cm^{-3}) and rf power (5 W) are kept fixed. At $V_b \sim +38$ V, the void radius is minimum which indicates that pin bias is very close to the plasma potential. This observation can be utilized as a diagnostic tool for plasma potential measurement which is often missed by the Langmuir probe in the rf discharge. With the decrease

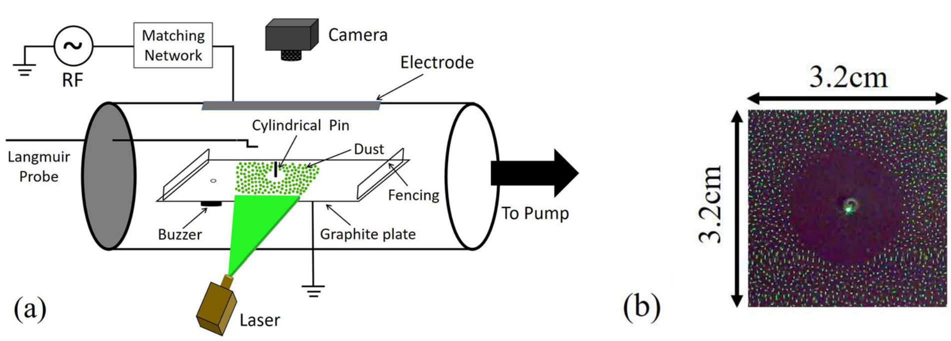

FIG. 1. (a) Schematic diagram of the experimental setup. (b) A typical image showing the top view of the dust layer (3.2 cm × 3.2 cm), with the void center at the pin position. The pin is at floating potential, $V_f = 2V$. rf power = 5 W, Ar pressure ∼ 4.6 Pa.

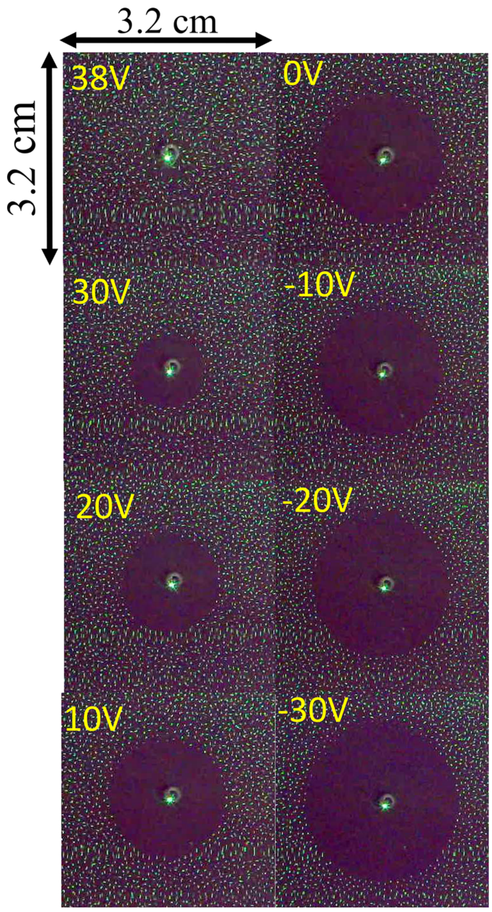

FIG. 2. Images showing top view of dust void at different pin bias voltages $V_b = 38$ V to -30 V. The dimension of each image is 3.2 cm × 3.2 cm. rf power = 5 W, Ar pressure ∼4.6 Pa. A strip with elongated dust particles in the lower half of each image is due to defects in the glass chamber.

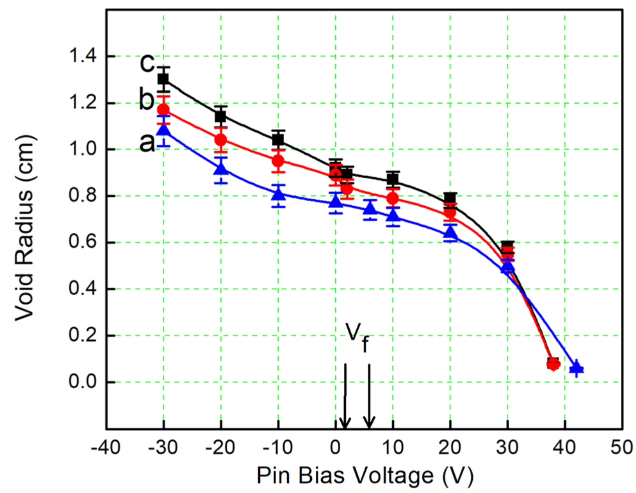

FIG. 3. Measured void radii as a function of pin bias voltage at different pressures, a ∼ 2.6 Pa, b ∼ 4.6 Pa, and c ∼ 5.3 Pa; V_f denotes the pin bias equal to its floating potential. rf power = 5W.

in the pin bias with respect to the plasma potential, the void radius increases. The radius of the void is measured to be ∼1.2 cm for pin bias $V_b = -30$ V. It is, therefore, clear that the sheath potential arising out of difference between the V_b and the plasma potential V_{plasma} determines the size of the void around the pin.

We also observe that the void size varies with neutral gas pressure. To investigate the effect of neutral pressure/density, the void radius is measured as a function of pin bias (V_b) for three different Ar pressures. The pressure range selected for the investigation is below the phase transition region (2.6 Pa to 5.3 Pa). In our experiment, crystallization occurs above a neutral pressure of 6 Pa. Typical results are shown in Fig. 3. At the beginning, a certain number density of dust particles ∼600 cm^{-3} at neutral pressure of 2.6 Pa is dispersed into the plasma. The discharge rf power is fixed at 5 W. The Ar neutral pressure is then slowly increased keeping dust number density and rf power unaltered. It is observed that for a fixed pin bias ($V_b < V_{plasma}$), the void size increases slightly with the increase in gas pressure from 2.6 Pa to 5.3 Pa. We also observe a decrease in the interparticle distance with an increase in the neutral pressure which in turn increases the dust density (600–1100 cm^{-3}). It is well known that an increase in neutral pressure increases the coulomb interaction potential of the dust particles and also reduces the dust thermal energy leading to strong coupling and crystallization. The normal plasma parameters such as plasma density and electron temperature do not change appreciably in this pressure range.[32] We also found that the floating potential of the pin can be easily obtained by comparing the void size under equivalent bias conditions. At neutral pressure 2.6 Pa, the measured void radius (0.7 cm) at $V_b = 6$ V is found to be the same as that measured at the floating condition. This indicates that 6 V is the floating potential of the pin (V_f) at pressure 2.6 Pa. Similarly, at a neutral pressure of 4.6 Pa and 5.3 Pa, we find that the floating potential of the pin can be correctly obtained corroborating the measured void radius. In Fig. 3, observed V_f at each pressure is indicated by arrow marks.

The dust void, so produced around the pin, is due to the force balance between the outward electric field force (F_e) and the inward ion drag force (F_i) on the dust particle. To estimate the strength of the forces, we first calculated the sheath potential $V_s(r)$ profile around the pin at different pin bias conditions using the Debye sheath model. The sheath electric field $E(r)$ profile is then obtained. As the size of the pin (100 μm diameter) is very small, we consider the pin as a point charge and so, according to the Debye sheath model,[33,34] the potential from the pin falls off as

$$V_s(r) = V_s \exp(-r/\lambda_{De}) + V_{plasma}, \quad (1)$$

where $V_s(r)$ is the sheath potential at a distance "r" from the pin, $V_s = (V_b - V_{plasma})$, λ_{De} is the electron Debye length, and V_{plasma} is the plasma potential. An example of potential profiles around the pin when it is biased from -30 V to $+30$ V is shown in Fig. 4(a). The inset graph shows an enlarged view of the potential profiles for the marked rectangular box. The measured values of V_{plasma} and V_f are 38 V and 2 V, respectively. When bias on the pin is increased from –30 V to 38 V, the potential difference between the pin and plasma (V_s) varies from –68 V to 0 V. The corresponding electric field profiles $E(r)$ are obtained by differentiating the potential profiles for different pin voltages. Figure 4(b) shows

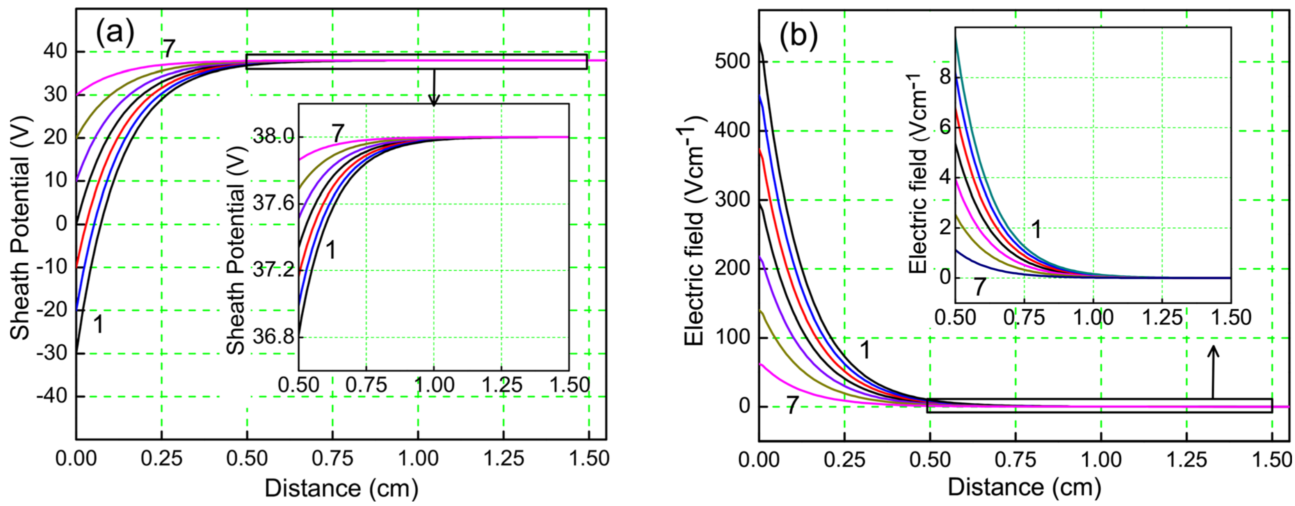

FIG. 4. Theoretical (a) sheath potential profiles and (b) electric field profiles for different pin bias voltages. The curves 1 to 7 correspond to pin bias –30 V to +30 V in a step of 10 V. The distance is measured from the pin. The inset graphs show profiles for the marked areas. Ar pressure ~ 4.6 Pa, rf power = 5 W, and plasma potential = 38 V.

$E(r)$ profiles obtained from potential curves shown in Fig. 4(a). The enlarged view of the $E(r)$ profile for the marked area is shown in the inset graph. The electric field values, $E(r_0)$ at different void boundary positions (r_0), are obtained from the respective $E(r)$ profiles.

The electric field force F_e on the dust particles is then calculated by using the relation

$$F_e = Q_d E(r_0), \tag{2}$$

where $Q_d (= Z_d e)$ is the charge on the dust particle (Z_d is the dust charge number) and $E(r_0)$ is the electric field value at void boundary position r_0. The average charge Q_d on a dust particle is calculated from the force balance between upward sheath electrostatic force above the plate ($Q_d E_h$, where E_h is the electric field at levitation height h) and downward gravitational force ($m_d g$, where g is the acceleration due to gravity). In an earlier experiment (in the same device), the vertical sheath potential profile (from bulk plasma to the plate) is measured using an emissive probe.[32] The sheath electric field is then obtained from the potential profile. At a typical dust levitation height of ~ (0.7–1.0) cm, the measured sheath electric field E_h is found to be ~(4–5) V cm^{-1}. The dust charge is then calculated using the relation $Q_d = m_d g/E_h$ and is found to be $\sim 3.23 \times 10^{-15}$ to 4.11×10^{-15} Coulomb ($\sim 10^4$ e) for the present experimental condition. The Q_d value obtained as such closely agrees with the dust charge calculated by using the Orbital Motion Limited (OML) theory. In another experiment, Nakamura and Ishihara also measured the average dust charge on a 5 μm diameter particle of the order of $\sim 10^4$ e under similar experimental conditions.[35]

Using the measured value of Q_d and $E(r_0)$ from the Debye sheath model, F_e is calculated at different void boundaries and it is on the order of 10^{-13} N. In the case of vertical levitation of dust particles, the upward electric field force required to balance the force due to gravity ($m_d g$, where m_d is the mass of the dust particle and g is the acceleration due to gravity) is one order larger ($\sim 10^{-12}$ N).

The ion drag force, which occurs due to the streaming of the ions relative to the dust particles, is usually expressed as a sum of the collection and the orbital forces[36,37]

$$F_i = F_{coll} + F_{orb}. \tag{3}$$

The collection force F_{coll} is associated with the momentum transfer from the ions that are collected by the grain and the orbital force F_{orb} occurs due to the momentum transfer from the ions that are elastically scattered in the electric field of the charged dust particle. According to the model given by Barnes *et al.*,[37] the collection force is given as

$$F_{coll} = m_i v_s n_i u_i \pi b_c^2, \tag{4}$$

where m_i and u_i are the ion mass and drift velocity, respectively. In addition, $v_s = \sqrt{{v_{th}}^2 + {u_i}^2}$ is the mean speed of the ions, where v_{th} is their thermal velocity, and $b_c = \sqrt{a^2\left(1 - 2e\varphi_f/m_i v_s^2\right)}$ is the critical parameter at which the ion hits the dust particle. Here, φ_f is the floating potential of the dust particle with respect to the plasma and a is the radius of the dust particle. Similarly, the orbital force due to Coulomb scattering is

$$F_{orb} = m_i v_s n_i u_i 4\pi b_{\pi/2}^2 \Gamma, \tag{5}$$

where $b_{\pi/2} = (Q_d e/4\pi\varepsilon_0 m_i v_s^2)$ and $\Gamma = \ln\sqrt{\left(\lambda_D^2 + b_{\pi/2}^2\right)/\left(b_c^2 + b_{\pi/2}^2\right)}$ are the impact parameter for 90° deflection and the Coulomb logarithm, respectively, and ε_0 is the absolute permittivity of free space. λ_D is the linearized Debye length $\lambda_D = (\lambda_{Di}^{-2} + \lambda_{De}^{-2})^{-1/2}$, where λ_{Di} and λ_{De} are the ion and electron Debye length, respectively. The value of λ_D is very close to the ion Debye length λ_{Di}. The ion drift velocity is given by $u_i = \mu E(r)$, where $\mu = e/m_i \nu_{in}$ is the ion mobility with $\nu_{in} \cong v_{th} n_n \sigma_{in}$ being the ion-neutral collision frequency, σ_{in} the momentum transfer cross-section for ion-neutral collisions, and n_n the neutral number density. The effective momentum transfer cross-section (σ_{in}) is $\sim 10^{-14}$ cm^2 taking into account both charge exchange and polarization interaction.[38,39] The value of ν_{in} increases from 1.6×10^5 s^{-1} to 3.2×10^5 s^{-1} when neutral pressure is varied from 2.6Pa to 5.3Pa. This indicates a decrease in ion drag force when neutral density is increased. The ion drag force is then obtained from Eq. (3) for all the void boundaries. The estimated values of F_e and F_i at various void boundaries associated with respective pin bias voltages are shown in Fig. 5 for three different neutral pressures 2.6, 4.6, and 5.3Pa. It is noted that force balance occurs at lower values and void expands when the neutral density is increased. The balance of the electric field force and the ion drag force accounts well for all the void sizes observed in the experiment.

The variation of F_e and F_i as a function of distance from the pin (r) is also obtained numerically for all the different pin bias voltages. A typical plot of the forces for pin voltage $V_b = 10$ V at 4.6 Pa is shown in Fig. 6. Inside the void or close to the pin, F_i is very small compared to F_e. At a certain distance from the pin, the magnitude of the two forces become equal. It is to be noted that F_e is directed outward and direction of F_i is inward. The intersection point of the curves accounts for the void boundary. Beyond this point, the two forces remain almost the same. This signifies that beyond the void boundary, the dust particles do not feel any net force thus forming a stable two dimensional dust layer. In this case, the balance point (i.e., the void boundary) is located at $\sim$0.69 cm from the pin, which almost matches with the experimentally observed void boundary $\sim$0.78 cm under the same experimental condition.

The void radius (r_0) corresponding to different pin bias voltages is obtained from the respective force versus distance plots (as shown in Fig. 6) and then compared with the experimentally observed values. A typical plot showing comparison of experimental values with theoretically obtained r_0 values for pin voltages from -30 V to $+38$ V at 4.6 Pa is shown in Fig. 7. It is seen that the theoretical estimation of

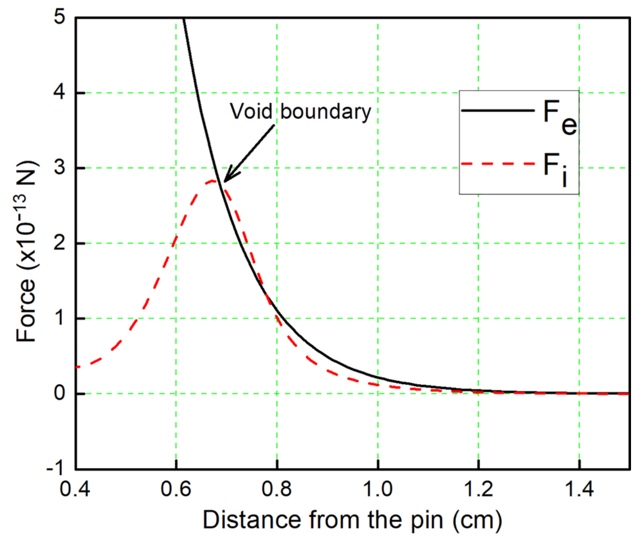

FIG. 6. Typical plot of electric field force F_e and ion drag force F_i as a function of distance from the pin. Ar pressure $\sim$ 4.6 Pa and pin bias voltage 10V. The balance point of the two forces is 0.69 cm from the pin which represents the void boundary.

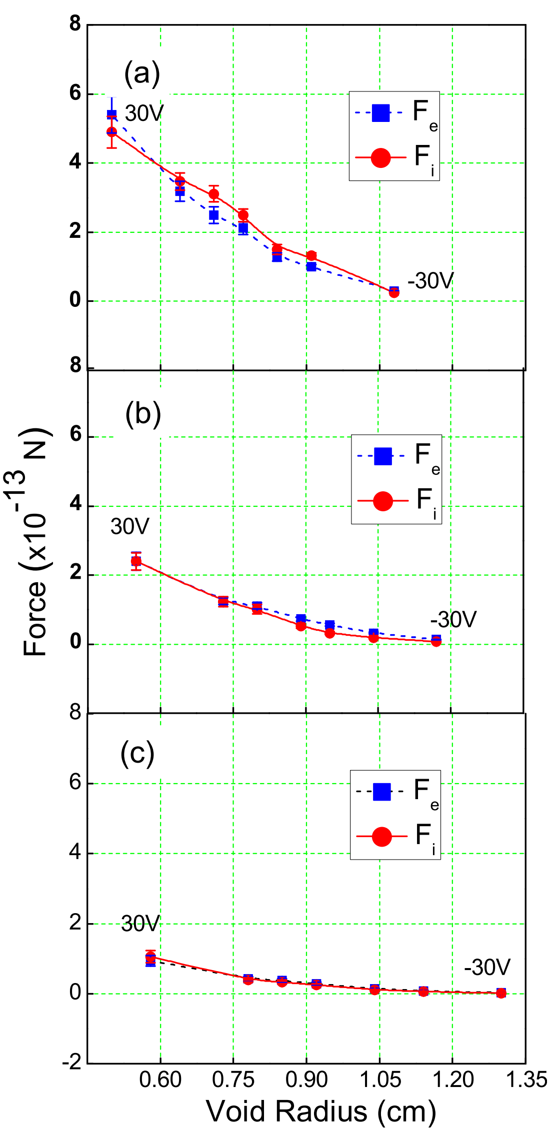

FIG. 5. Electric field force (F_e) and Ion Drag force (F_i) at void boundaries for different Ar pressures, (a) 2.6 Pa, (b) 4.6 Pa, and (c) 5.3 Pa.

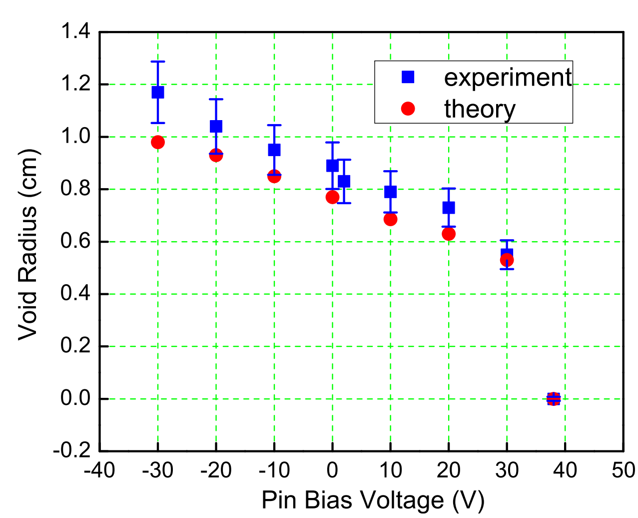

FIG. 7. Comparison of experimentally measured (blue squares) and theoretically obtained (red circles) void radius for different pin bias voltages. Ar pressure = 4.6 Pa and rf power = 5 W.

the void size for different pin bias voltages fits well with the experimental measurements. At higher sheath potentials (more negative pin bias voltage), the nonlinear sheath expansion contributes to slight differences with theoretical values of the void size.

Next, we examine the effect of dust density variation on the void structure formed around the pin at the floating potential (6 V). To do this, rf power (5 W) and Ar neutral pressure (2.6 Pa) are kept constant and dust density n_d is increased from 500 cm^{-3} to 1200 cm^{-3} (by injecting more particles from the buzzer). Typical images of void observed at five different n_d values are shown in Fig. 8. It is clearly observed in the images that the void radius decreases with increasing dust density. The void radii at different dust densities are measured from the images and are plotted in Fig. 9. The electric field values $E(r_0)$ at the void boundary which are obtained from the field profiles derived from the Debye sheath model [as shown in Fig. 3(b)] are also shown in Fig. 9 for different dust density conditions. It is found that the void radius decreases from 1.20 cm to 0.77 cm for dust density increment from 500 cm^{-3} to 1200 cm^{-3} at constant Ar pressure.

The variation in the dust density modifies the charge neutrality as well as the dust charging process.[40] Therefore, the value of average charge per dust changes depending on the number density of dust. Incorporating the Havnes parameter P, defined as $P = (n_d Z_d/n_i) = (4\pi\epsilon_0 a k_B T_e/e^2) \times (n_d/n_i)$, where n_i is the ion density and k_B is the Boltzmann constant, in the OML theory to estimate average dust charge, we get the following expression for the normalized dust floating potential $\hat{\varphi}$:

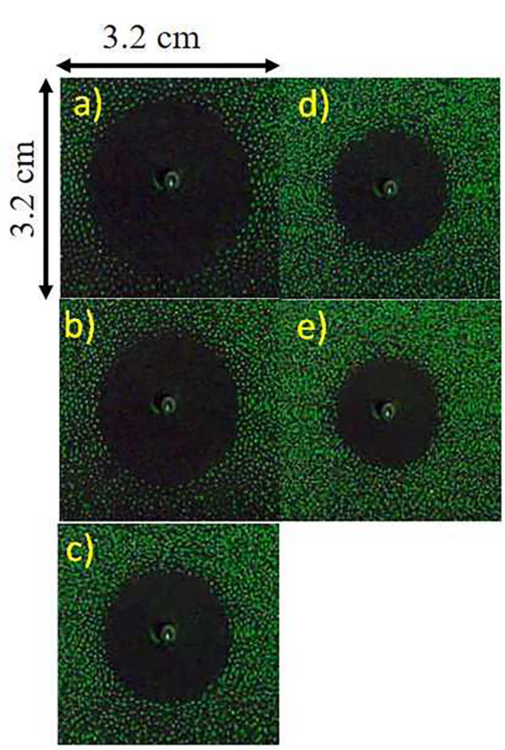

FIG. 8. Images showing top view of void at different dust densities, (a) 500 cm^{-3}, (b) 700 cm^{-3}, (c) 800 cm^{-3}, (d) 1000 cm^{-3}, and (e) 1200 cm^{-3}. The dimension of each image is 3.2 cm × 3.2 cm. Ar pressure = 2.6 Pa, rf power = 5 W, and pin at floating potential (6 V).

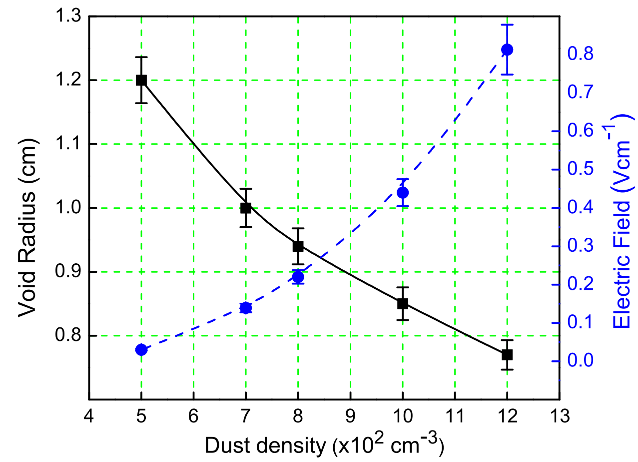

FIG. 9. Measured void radius (black squares) and $E(r_0)$ (blue circles) at different dust densities. Pressure ~ 2.6 Pa, rf power = 5 W, and pin floating potential = 6 V.

$$\exp(-\hat{\varphi}) = (1 - \hat{\varphi} P)^{-1} \sqrt{\frac{m_e}{m_i \tau}} (1 + \hat{\varphi}\tau), \tag{6}$$

where $\hat{\varphi} = e\varphi_f/k_B T_e$, $\tau = T_e/T_i$, m_e and m_i are the electron and ion mass, respectively, and T_i is the ion temperature. Here, the quasineutrality condition $n_e/n_i = 1 - P\hat{\varphi}$ is used with the assumption that the ion density n_i does not change when the dust density is varied. Using our typical experimental parameters, i.e., ion density $n_i \sim 10^{14}$ m^{-3}, $T_e \sim 6$ eV, and $T_i \sim 0.03$ eV at 2.6 Pa in Eq. (6), the normalized dust floating potential $\hat{\varphi}$ versus Havnes parameter P is plotted and is shown in Fig. 10. We consider that charge neutrality is affected through electron depletion when the dust density is increased, while the ion density remains unaltered. For $P \sim 0$, the maximum value of the dust floating potential corresponds to isolated dust particles. Here, the interparticle distance is much larger than the Debye length. When $P \sim 1$, the dust density is considerably high and the inter particle distance becomes smaller than the Debye length. Under this situation, the average dust charge reduces which in turn decreases the dust floating potential. For a higher value of P

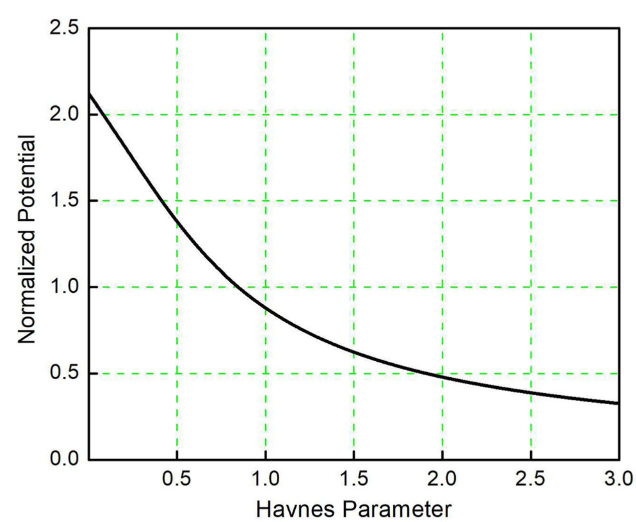

FIG. 10. Normalized dust floating potential $\hat{\varphi}$ as a function of Havnes Parameter P obtained by using Eq. (6). $\tau = 200$.

($>$1), the average dust charge reduces further and the dust floating potential decreases significantly. For dust density variation in the range of 500 cm^{-3} to 1200 cm^{-3}, the value of P varies from 0.05 to 0.12. In this range, the normalized dust floating potential $\hat{\varphi}$ changes from 2.04 to 1.93. The dust charge is then calculated by using the relation $\hat{\varphi} = e\varphi_f/k_B T_e = Z_d e^2/4\pi\epsilon_0 a k_B T_e$, for the present dust density variation range (i.e., for $P \sim 0.05$ to 0.12) and we found a very slight decrease in the Z_d value from 2.13×10^4 to 2.02×10^4 e. Thus, the electric field force $F_e = Q_d E(r_0)$ is calculated at different void boundary positions r_0 with varying dust density n_d.

Dust density variation also has an impact on the ion drag force in a strongly coupled complex plasma.[31] The increase in the dust density decreases the interparticle distance and this limits the impact parameter for ion scattering, thus affecting the cross-section for ion and dust particle collisions. The effective scattering cross-section in the ion dust collisions is defined as

$$\sigma_{eff}^{-1} = \sigma_{id}^{-1} + \frac{4}{\pi\Delta^2}, \tag{7}$$

where $\sigma_{id} = 4\pi b_{\pi/2}^2 \Gamma$ is the scattering cross-section for an individual dust particle and the second term is a cross-section corresponding to the largest admissible impact parameter for ions $\sim \Delta/2$ [Δ is the average interparticle distance given as $\Delta = (3/4\pi n_d)^{1/3}$]. Thus, taking this effect into account, there would be a slight modification in the ion drag force [Eq. (3)]. Inserting the above expression of σ_{eff}^{-1} [Eq. (7)] into the collection and orbital forces from Eqs. (4) and (5), respectively, ion drag force F_i is obtained as

$$F_i \cong m_i v_s n_i u_i \left(\pi b_c^2 + \frac{\sigma_{id}}{\left(1 + \frac{4\sigma_{id}}{\pi\Delta^2}\right)} \right). \tag{8}$$

The ion flow velocity is again calculated from the mobility equation $u_i = (e/m_i \nu_{in})E(r_0)$ at particular void boundary positions (r_0). At each dust density, snapshots are taken and the images are analyzed to obtain the average interparticle distance. For $n_d \sim 500$ to 1200 cm^{-3}, the interparticle distance decreases from 7.81×10^{-2} cm to 5.83×10^{-2} cm. Considering that the dust charge decreases slightly with the increase in the dust density, the ion dust scattering cross-section σ_{id} is calculated and is observed that $\sigma_{eff} = \sigma_{id}/\left(1 + \frac{4\sigma_{id}}{\pi\Delta^2}\right)$ decreases with increasing n_d. Consequently, the ion drag force F_i is calculated at the respective void boundary positions r_0 from Eq. (8) and is compared with the electric field force F_e at the corresponding values of r_0. A plot of electric field force and the ion drag force at different void boundary positions corresponding to different dust densities is shown in Fig. 11. It is observed that both the forces balance well at different void boundaries corresponding to different n_d values. Individually, both the forces decrease slightly with the increase in dust density; however, the decrease in the void size with the increase in dust density is attributed to the increase in ion drag force. Our results are consistent with the theoretical consideration proposed by Yaroshenko *et al.*[31]

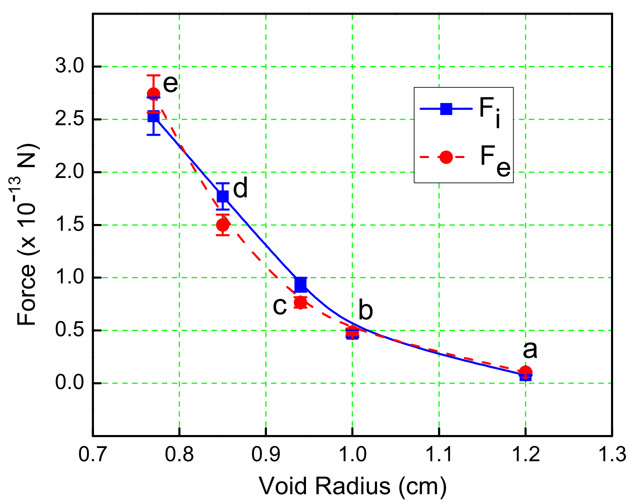

FIG. 11. Calculated electric field force (F_e) and ion drag force (F_i) at different void boundaries corresponding to the dust densities a—500 cm^{-3}, b—700 cm^{-3}, c—800 cm^{-3}, d—1000 cm^{-3}, and e—1200 cm^{-3}.

IV. CONCLUSIONS

Dust void in a strongly coupled dusty plasma, created by inserting a cylindrical pin of very small diameter into an rf discharge argon plasma, has been studied. The void is formed due to balance of two oppositely directed dominating forces, outward electric field force and inward ion drag force acting on the dust particles. The sheath electric field around the pin plays the key role in determining the force balance and void appears only when the pin is biased below the plasma potential. Void disappears when the pin is biased at plasma potential, providing an authentic way to estimate the plasma potential. With the decrease in pin bias with respect to plasma potential, the sheath potential increases resulting in an increase in the outward electric field force on the particles. With the increase in neutral pressure, the mobility and flow velocity of ions decrease which in turn reduces the ion drag force resulting in a larger void size. The electric field around the pin is estimated by using the Debye sheath model. Consequently, the electric field forces and ion drag forces on the dust particles are calculated at different void boundaries corresponding to different pin bias voltages. At all the boundaries, the two forces balance each other. The characteristics of the void size are also studied with the variation of dust density and are observed that the void radius decreases with increasing dust density. The force balance condition at respective void boundaries is also verified in this case. The decrease in the void size with increasing dust density is consistent with the theoretical considerations proposed by Yaroshenko *et al.*[31] and is attributed to the increase in the ion flow velocity. It is also found that the electric field force required for vertical levitation of dust particles is one order higher compared to that at the void boundary created in the horizontal direction. This indicates that vertical balance of dust particles occurs deep inside the presheath region of the sheath where the electric field is one order higher. The characteristics of the voids formed in dusty plasma play a vital role in various dust collective processes and would help in understanding structures associated with dust flows past an obstacle.

ACKNOWLEDGMENTS

The authors would like to thank Mr. Bidyut Chutia for assistance during the experiment. One of the authors (Y.B.) thanks the DST-INSPIRE, Government of India, for financial support.

[1]P. Bliokh, V. Sinitsin, and V. Yaroshenko, *Dusty and Self-Gravitational Plasmas in Space* (Kluwer Academic Publishers, Dordrecht, 1995).
[2]D. A. Mendis and M. Rosenberg, IEEE Trans. Plasma Sci. **20**, 929 (1992).
[3]R. L. Merlino, "Dusty plasmas and applications in space and industry," *Plasma Physics Applied* (Transworld Research Network, Kerala, India, 2006), pp. 73–110.
[4]Y. Nakamura, *New Developments in Nuclear Fusion Research* (Nova Science Publishers, 2006).
[5]C. K. Goertz, Rev. Geophys. **27**, 271, https://doi.org/10.1029/RG027i002p00271 (1989).
[6]D. A. Mendis and M. Rosenberg, Annu. Rev. Astron. Astrophys. **32**, 419 (1994).
[7]F. Verheest, *Waves in Dusty Space Plasmas* (Kluwer Academic Publishers, Dordrect, 2000).
[8]G. S. Selwyn, J. E. Heidenreich, and K. L. Haller, J. Vac. Sci. Technol. A **9**, 2817 (1991).
[9]V. E. Fortov, A. V. Ivlev, S. A. Khrapak, A. G. Khrapak, and G. E. Morfill, Phys. Rep. **421**, 1–103 (2005).
[10]S. Ghosh, T. K. Chaudhuri, S. Sarkar, M. Khan, and M. R. Gupta, Astrophys. Space Sci. **278**, 465 (2001).
[11]P. K. Shukla, Phys. Plasmas **8**, 1791 (2001).
[12]P. K. Shukla and A. A. Mamun, *Introduction to Dusty Plasma Physics* (Institute of Physics, Bristol, 2002).
[13]S. K. Sharma, A. Boruah, and H. Bailung, Phys. Rev. E **89**, 013110 (2014).
[14]A. Boruah, S. K. Sharma, H. Bailung, and Y. Nakamura, Phys. Plasmas **22**, 093706 (2015).
[15]S. K. Sharma, A. Boruah, Y. Nakamura, and H. Bailung, Phys. Plasmas **23**, 053702 (2016).
[16]H. Thomas, G. E. Morfill, V. Demmel, J. Goree, B. Feuerbacher, and D. Mohlmann, Phys. Rev. Lett. **73**, 652 (1994).
[17]H. Ikezi, Phys. Fluids **29**, 1764 (1986).
[18]J. H. Chu and I. Lin, Phys. Rev. Lett. **72**, 4009 (1994).
[19]D. Samsonov, J. Goree, Z. W. Ma, A. Bhattacharjee, H. Thomas, and G. E. Morfill, Phys. Rev. Lett. **83**, 3649 (1999).
[20]P. Bandyopadhyay, R. Dey, and A. Sen, Phys. Plasmas **24**, 033706 (2017).
[21]G. Praburam and J. Goree, Phys. Plasmas **3**, 1212 (1996).
[22]D. Samsonov and J. Goree, Phys. Rev. E **59**, 1047 (1999).
[23]G. E. Morfill, H. Thomas, U. Konopka, H. Rothermel, M. Zuzic, A. Ivlev, and J. Goree, Phys. Rev. Lett. **83**, 1598 (1999).
[24]H. Rothermel, T. Hagl, G. E. Morfill, M. H. Thoma, and H. M. Thomas, Phys. Rev. Lett. **89**, 175001 (2002).
[25]A. V. Fedoseev, G. I. Sukhinin, M. K. Dosbolayev, and T. S. Ramazanov, Phys. Rev. E **92**, 023106 (2015).
[26]V. V. Shumova, D. N. Polyakov, and L. M. Vasilyak, Plasma Sources Sci. Technol. **26**, 035011 (2017).
[27]R. P. Dahiya, G. V. Paeva, W. W. Stoffels, E. Stoffels, G. M. W. Kroesen, K. Avinash, and A. Bhattacharjee, Phys. Rev. Lett. **89**, 125001 (2002).
[28]J. Goree, G. E. Morfill, V. N. Tsytovich, and S. V. Vladimirov, Phys. Rev. E **59**, 7055 (1999).
[29]C. O. Thompson, N. D'Angelo, and R. L. Merlino, Phys. Plasmas **6**, 1421 (1999).
[30]E. Thomas, Jr., K. Avinash, and R. L. Merlino, Phys. Plasmas **11**, 1770 (2004).
[31]V. V. Yaroshenko, S. A. Khrapak, and G. E. Morfill, Phys. Plasmas **20**, 043703 (2013).
[32]S. K. Sharma, R. Kalita, Y. Nakamura, and H. Bailung, Plasma Sources Sci. Technol. **21**, 045002 (2012).
[33]K. M. Frederick-Frost and K. A. Lynch, Phys. Plasmas **14**, 123503 (2007).
[34]G. Livadiotis and D. J. McComas, J. Plasma Phys. **80**, 341 (2014).
[35]Y. Nakamura and O. Ishihara, Phys. Plasmas **16**, 043704 (2009).
[36]A. Melzer, *Introduction to Colloidal (Dusty) Plasmas*, Lecture Notes (Institute fur Physik, Ernst-Moritz-Arndt-Universitat, Greifswald, 2005).
[37]M. S. Barnes, J. H. Keller, J. C. Forster, J. A. O'Neill, and D. K. Coultas, Phys. Rev. Lett. **68**, 313 (1992).
[38]M. A. Biondi and L. M. Chanin, Phys. Rev. **94**, 910 (1954).
[39]R. N. Varney, Phys. Rev. **88**, 362 (1952).
[40]O. Havnes, C. K. Goertz, G. E. Morfill, E. Grun, and W. Ip, J. Geophys. Res. **92**, 2281, https://doi.org/10.1029/JA092iA03p02281 (1987).